Author's response to Review1

The responses are organized according to the organization of the questions. When necessary, the beginning of the question is repeated.

- *The choice of the altitudinal beta-factors is crucial. How sensitive is the optimization to the choice of initial beta values?[...]*
  In order to answer this question in the paper, the text from P11L333 to P12L335 is remplaced by the following text :
  The optimization method is highly sensitive to the choice of inital values for the β_1, β_2, β_3, z1 and z2 parameters. Several attempts have been done and the choices presented TABLE 6 are justified by the following arguments :

  - Minimum and maximum values for the altitude thresholds z1 and z2 are chosen accordingly to both litterature review (Barros et al., 2000; Anders et al., 2006; Bookhagen and Burbank, 2006; Shrestha et al., 2012; Nepal, 2012; Savéan, 2014) and observations. The first inquired altitudinal threshold is described in litterature between 2000 m and 3000 m and the second threshold is described above 4000 m. These intervals have been enlarged to also test related values.

  - Maximum (resp. minimum) value for β_1 (resp. β_2) are chosen about 10 times larger than the value computed based on observation. Considering the definition of the beta coefficient, a value greater than 2 km^{-1} (resp. lower than -2 km^{-1}) would lead to a multiplication of precipitation by 1.22 (resp. by 0.82) within 100 m. When applied to the precipitation oberved at stations, this would lead to inconsistent precipitation when increasing altitude by 100 m.

  - The β_3 coefficient has to be negative because a positive value would lead to unrealistic values at high altitudes. Moreover, the minimum value is chosen to be significantly smaller than the value computed for β_3 based on the observations, but also to remain higer than the value computed for β_2 based on the observations.

- *it is stated that the precipitation analysis has been done by applying an IDW scheme. On which grid resolution is it done?*
  The IDW interpolation is performed over a 1 km resolution grid. This is specified P9L255. Consequently, the manuscript is not modified concerning this point.

- *[...]Why did the authors not use ECO-CLIMAP2 data?*
  The ECOCLIMAP2 product is only available for Europe (see (Faroux et al., 2013)). The studied area is not covered by ECOCLIMAP2. The following sentence is inserted P11L352 :
  The ECOCLIMAP2 product (Faroux et al., 2013) is derived from ECOCLIMAP1 and provides enhanced descriptions of surfaces. However, ECOCLIMAP2 is only available over Europe and therefore is not used in this study.

- *Minor remarks*
  The minor remarks are corrected in the manuscript :

  - P3L107 : these stations are presented TABLE 2

  - P7L201-202 : The descreasing of precipitation with altitude is characterized

  - P12L344 : Based on values

  - *P4L121 : replace "aleatory" by "random"*
    I agree that the term 'random' would be more grammatically correct here. However, the term 'aleatory' is chosen in order to match the classification of uncertainties proposed by Beven,2016. In (Beven, 2015), aleatory error is defined as 'uncertainty with stationary statistical characteristics. May be structured (bias,autocorrelation, long term persistence) but can be reduced to a stationary random distribution'. Consequenly, I won't modify this point in the manuscript.

- *P12L349-362 : What are behavioral and nonbehavioral parameter sets ? Please explain more detailed.*

Behavioral parameter sets are defined P9L248 : A behavioral parameter set is a set that respects conditions (maximum or minimum thresholds) on the output of the orographic precipitation model. At P12L338, the following sentence is inserted in the manuscript : A behavioral parameter set is a set that leads to an annual amount of total precipiation for both catchments comprised between the minimal and maximal values presented Table7. A parameter sets that does not meet these conditions is considered as non-behavioral.

- *The years 2013 and 2014 are used as spin-up period. Why such a long spin-up time ? ?*
The hydrological year that runs from April,1st 2013 to March, 31rd 2014 (i.e. 365 days) is used as spin-up period. 365 days are considered to be a necessary spin-up period to set up all reservoirs at a representative volume, in particular for snow pack and soil water storage. P13L373 , the following sentence is added : The 2013–2014 hydrological year was used [...]

Author's response to Review2

The responses are organized according to the organization of the questions. Extracts of the questions are repeated and the answers are introduced by (*).

- *Only one IDW is chosen for interpolation of precipitation[. . .]. They should try to look for such method that is called non-deterministic i.e. geostatistical methods.*

An important review of interpolation method suitable for mountainous areas has been done. In particular, three of the co-authors have applied the cokriging geostatistical interpolation method to estimate the monsoon precipitation in the Koshi River basin (**?**) . In order to answer this question in the paper, the following text is inserted P7L192 :
However, few studies provide precipitation fields at the hourly time scale (**??**) and precipitation fields at spatial scales lower than 1 km are always obtained using altitude linear lapse rates (**???**). However, the considered lapse rates are constant in time and/or uniform in space. The spatial and temporal variability of the precipitation is then not represented in these studies. Moreover, the geostatistical cokriging method has been applied by **?** for monsoon precipitation interpolation over the Koshi catchment. However, the provided precipitation fields overally underestimate the observations, and this method is shown not to be adequate for the interpolation of solid precipitation.

and the following text is inserted P7L192 :
This method presents the advantage of using an altitudinal factor which can vary in time and space. The spatial and temporal variability of the precipitation is therefore represented in this method. Moreover, the effect of altitude is independently studied and the controlling parameters have physical meaning.

- *Table 1 should be deleted ; it is not cited in the text*
The reference to TABLE 1 is added P5L106.

- *P4L121 : I don't understand "Local measurements are necessarily biased by aleatory errors".*
For a better understanding, this sentence is reformulated as : 'Local measurements can not be an exact quantification of any climatic variables, and they are necessarily associated by errors that follow an random distribution law. ' A large number of factor can indeed affect local measurements of climatic variables (e.g. approximation in the sensor records, influence of variations faster that the time step, local site effects, . . .).

- *P4, L124 replace aleatory by random*
  I agree that the term 'random' would be more grammatically correct here. However, the term 'aleatory' is chosen in order to match the classification of uncertainties proposed by Beven,2016. In Beven,2016, aleatory error is defined as 'uncertainty with stationary statistical characteristics. May be structured (bias,autocorrelation, long term persistence) but can be reduced to a stationary random distribution'. Consequenly, I won't modify this point in the manuscript.

- *P4, L131-134 : difficult to understand, please rearrange your sentence again*
  This sentence is modified as :
  Water level time series are available from March 2014 to March 2015. Time serie at Kharikhola station contains 34% of missing data in 2014–2015, corresponding to damages to the sensor.

Bibliographie

Anders, A.M., et al., 2006. Spatial patterns of precipitation and topography in the himalaya. Geological Society of America Special Papers, 398, 39–53.

Barros, A., et al., 2000. A study of the 1999 monsoon rainfall in a mountainous region in central nepal using trmm products and rain gauge observations. Geophysical Research Letters, 27 (22), 3683–3686.

Beven, K., 2015. Facets of uncertainty : epistemic uncertainty, non-stationarity, likelihood, hypothesis testing, and communication. Hydrological Sciences Journal, (just-accepted).

Bookhagen, B. and Burbank, D.W., 2006. Topography, relief, and trmm-derived rainfall variations along the himalaya. Geophysical Research Letters, 33 (8). Available from : http ://dx.doi.org/10.1029/2006GL026037.

Faroux, S., et al., 2013. Ecoclimap-ii/europe : a twofold database of ecosystems and surface parameters at 1 km resolution based on satellite information for use in land surface, meteorological and climate models. Geoscientific Model Development, 6 (2), 563–582.

Nepal, S., 2012. Evaluating upstream-downstream linkages of hydrological dynamics in the himalayan region. Thesis (PhD). PhD Thesis. Friedrich Schiller University, Germany.

Savéan, M., 2014. Modélisation hydrologique distribuée et perception de la variabilité hydroclimatique par la population du bassin versant de la dudh koshi (népal). Thesis (PhD). Université de Montpellier 2.

Shrestha, D., Singh, P., and Nakamura, K., 2012. Spatiotemporal variation of rainfall over the central himalayan region revealed by trmm precipitation radar. Journal of Geophysical Research : Atmospheres, 117 (D22).

1

Providing a non-deterministic representation of spatial variability of precipitation in the Everest region.

Judith Eeckman[a], Pierre Chevallier[a], Aaron Boone [b], Luc Neppel [a], Anneke De Rouw [c], Francois Delclaux [a], Devesh Koirala [d]

[a]Laboratoire HydroSciences (CNRS, IRD, Universite de Montpellier) CC 57 - Universite de Montpellier 163, rue Auguste Broussonnet 34090 Montpellier, France;
[b]CNRM UMR 3589, Meteo-France/CNRS, Toulouse, France;
[c]Institut de Recherche pour le Developpement, Universite Pierre et Marie Curie, 4 place Jussieu, 75252 Paris cedex 5, France;
[d]Nepal Academy of Science and Technology GPO box: 3323 Khumaltar, Lalitpur, Nepal

ABSTRACT
This paper provides a new representation of the effect of altitude on precipitation that represent spatial and temporal variability of precipitation in the Everest region. Exclusive observation data are used to infer a piecewise linear function for the relation between altitude and precipitation and significant seasonal variations are highlighted. An original ensemble approach is applied to provide non deterministic water budgets for middle and high mountain catchments. Physical processes at the soil-atmosphere interface are represented through the ISBA surface scheme. Uncertainties associated with the model parametrization are limited by the integration of in-situ measurements of soils and vegetation properties. Uncertainties associated with representation of the orographic effect are shown to account for up to 16% of annual total precipitation. Annual evapotranspiration is shown to represent $26\% \pm 1\%$ of annual total precipitation for the mid-altitude catchment and $34\% \pm 3\%$ for the high-altitude catchment. Snow fall contribution is shown to be neglectible for the mid-altitude catchment and it represents up to $44\% \pm 8\%$ of total precipitation for the high-altitude catchment. These simulations at the local scale enhance current knowledge of the spatial variability of hydro-climatic processes in high- and mid-altitude mountain environments.

1. Introduction

The central part of the Hindu Kush Himalaya region presents tremendous heterogeneity, in particular in terms of topography and climatology. The terrain ranges from the agricultural plain of Terai to the highest peaks of the world, including Mount Everest, over a south-north transect about 150km long (FIGURE 1).

Two main climatic processes at the synoptic scale are distinguished in the Central Himalayas (Barros *et al.* 2000, Kansakar *et al.* 2004). First, the Indian Monsoon is

Judith Eeckman judith.eeckman-poivilliers@univ-montp2.fr

formed when moist air arriving from Bay of Bengal is forced to rise and condense on the Himalayan barrier. Dhar and Rakhecha (1981) and Bookhagen and Burbank (2010) assessed that about 80% of annual precipitation over the Central Himalayas occurs between June and September. However, the timing and intensity of this summer monsoon is being reconsidered in the context of climate change (Bharati *et al.* 2016). The second main climatic process is a west flux that gets stuck in adequately oriented valleys, and occurs between January and March. Regarding high altitudes (> 3000 m), this winter precipitation can occur exclusively in solid form and can account for up to 40% of annual precipitation (Lang and Barros 2004) with considerable spatial and temporal variation.

At a large ~~spatio temporal~~ spatio-temporal scale, precipitation patterns over the Himalayan range are recognized to be strongly dependent on topography (Anders *et al.* 2006, Bookhagen and Burbank 2006, Shrestha *et al.* 2012). The main thermodynamic process is an adiabatic expansion when air masses rise, but, at very high altitudes (> 4000 m), the reduction of available moisture is a concurrent process. ~~Altitudinal~~ Altitude thresholds of precipitation can then be discerned (Alpert 1986, Roe 2005). However, this representation of orographic precipitation has to be modulated considering the influence of such a protruding relief (Barros *et al.* 2004).

Products for precipitation estimation currently available in this area, e.g. the APHRODITE interpolation product (Yatagai *et al.* 2012) and the TRMM remote product (Bookhagen and Burbank 2006), do not represent spatial and temporal variability of orographic effects at a resolution smaller than 10 km (Gonga-Saholiariliva *et al.* 2016). Consequently, substantial uncertainty remains in water budgets simulated for this region, as highlighted by Savéan *et al.* (2015). In this context, ground-based measurements condensed in small areas have been shown to enhance the characterization of local variability of orographic processes (Andermann *et al.* 2011, Pellicciotti *et al.* 2012, Immerzeel *et al.* 2014). However, even if the Everest region is one of the most closely monitored areas of the Himalayan range, valuable observations remain scarce. In particular, the relation between altitude and precipitation is still poorly documented.

The objective of this paper is to provide a representation of the effect of altitude on precipitation that represent spatial and temporal variability of precipitation in the Everest region. The parameters controlling the shape of the altitudinal factor are constrained through an original sensitivity analysis step. Uncertainties associated with variables simulated through the ISBA surface scheme (Noilhan and Planton 1989) are quantified.

The first section of the paper presents the observation network and recorded data. The second section describes the model chosen to represent orographic precipitation, including computed altitude lapse rates for air temperature and precipitation. The method for statistical analysis through hydrological modeling is also described. The third section presents and discusses the results of sensitivity analysis and uncertainty analysis.

2. Data and associated uncertainties

### 2.1. *Meteorological station transect*

An observation network of ten stations (TABLE 1 and FIGURE 1) records hourly precipitation (P) and air temperature (T) since 2010 and 2014. The stations are equipped with classical rain gauges and HOBO ⓇR sensors for temperature. The stations are located to depict altitudinal profile of P and T over 1) the main river valley (Dudh Koshi valley), oriented south-north; 2) the Kharikhola tributary river, oriented east-west.

To reduce under-catching of solid precipitation, two Geonors ⓇR were installed at 4218 m and 5035 m in 2013. Measurements at Geonor ⓇR instrumentation allow to correct the effect of wind and the loss of snowflakes. Records from four other stations administrated by the EVK2-CNR association are also available. Total precipitation, air temperature, atmospheric pressure (AP), relative humidity (RH), wind speed (WS), short-wave radiation (direct and diffuse) (SW) and long-wave radiation (LW) have been recorded at the hourly time step since 2000 at Pyramid station (5035 m.a.s.l.). Overall, these ten stations cover an altitude range from 2078 m to 5035 m a.s.l., comprising a highly dense observation network, compared to the scarcity of ground-based data in this type of environment. The characteristics of the ten stations are summarized TABLE 1.

Table 1. Overview of the observation network used in this study. Air temperature (T), precipitation (P) atmospheric pressure (AP), relative humidity (RH), wind speed (WS), short- and long-wave radiation (SW, LW) are recorded at the hourly time scale. The Geonor ⓇR at the Pyramid and Pheriche stations record total precipitation P_{GEO} at the hourly time scale. The two hydrometric stations at Kharikhola and Pangboche record water level since 2014.

ID	Station	ALT m.a.s.l.	LAT	LON	Period		Measured variable
KHA	Kharikhola	2078	27.60292	86.70311	2014-05-03	2015-10-28	P,T
MER	Mera School	2561	27.60000	86.72269	2014-05-02	2015-10-28	P,T
BAL	Bhalukhop	2575	27.60097	86.74017	2014-05-03	2015-10-28	P,T
PHA	Phakding	2619	27.74661	86.71300	2010-04-07	2016-05-16	P,T
LUK	Lukla	2860	27.69694	86.72270	2002-11-02	2016-01-01	P,T
PAR	Paramdingma	2869	27.58492	86.73956	2014-05-03	2015-10-28	P,T
TCM	Pangom	3022	27.58803	86.74828	2014-05-03	2015-10-28	P,T
NAM	Namche	3570	27.80250	86.71445	2001-10-27	2016-01-01	P,T
PAN	Pangboche	3976	27.85722	86.79417	2010-10-29	2016-05-08	P,T
PHE	Pheriche	4218	27.89528	86.81889	2001-10-25	2016-01-01	T
					2012-12-06	2016-05-16	P_{GEO}
PYR	Pyramid	5035	27.95917	86.81333	2000-10-01	2016-01-01	T,AP,RH,WS, LW,SW
					2016-04-26	2016-04-26	P_{GEO}
668.7	Kharikhola	1985	27.60660	86.71847	2014-05-03	2016-05-20	Water level
668.03	Pangboche	3976	27.85858	86.79253	2014-05-17	2016-05-09	Water level

Annual means for temperature and preciptiation measured at these stations are presented are ~~presented~~ TABLE 2 for the two hydrological years 2014-2015 and 2015-2016. These time series ~~present~~ contain missing data periods, which can represent up to 61% ~~missing values~~ of the recorded period. For stations LUK, NAM, PHA, PAN, PHE and PYR, where relatively long time series are available, gaps were filled with the interannual hourly mean for each variable. For the other stations,
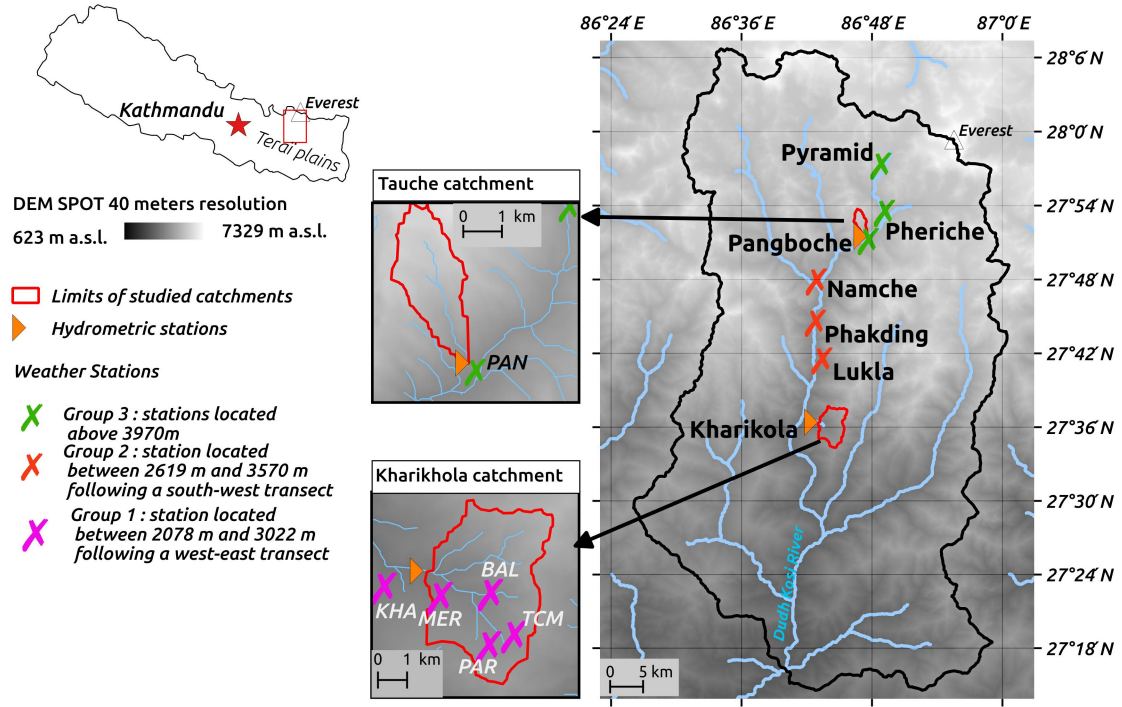
Figure 1. Map of the monitored area: the Dudh Koshi River basin at the Rabuwabazar station, managed by the Department of Hydrology and Meteorology, Nepal Government (station coordinates: $27°16'09''N$, $86°40'03''E$, station elevation: 462 m a.s.l., basin area: 3712 km2). The Tauche and Kharikhola subcatchments are defined by the corresponding limnimetric stations.

gaps were filled with values at the closest station, weighted by the ratio of mean values over the commun periods. Time series from 2013-01-01 to 2016-04-30 were then reconstructed from these observations.

Two seasons are defined based on these observations and knowledge of the climatology of the Central Himalayas: 1) the monsoon season, from April to September, including the early monsoon, whose influence seems to be increasing with the ~~recent~~ current climate change (Bharati *et al.* 2014); 2) the winter season, dominated by westerly entrances with a substantial ~~spatiotemporal~~ spatio-temporal variability.

Local measurements ~~are necessarily biased by aleatory errors (according to Beven (2015) uncertainty classification)~~ can not be an exact quantification of any climatic variables, and they are necessarily associated with errors that follow an random distribution law. In particular, snowfall is usually undercaught by instrumentation (Sevruk *et al.* 2009). However, since this study focuses most particularly on uncertainty associated with spatialization of local measurements, aleatory errors in measurements will not be considered here.

2.2. *Discharge measurement stations and associated hydrological catchments*

Two hydrometric stations were equipped with Campell® hydrometric sensors and encompass two sub-basins: Kharikhola catchment ($18.2\ km^2$) covers altitudes from 1900

m to 4450 m (mid-altitude mountain catchment) and Tauche catchment ($4.65 km^2$) altitudes range from 3700 m to 6400 m (high-altitude mountain catchment). Water level time series are available from March 2014 to March ~~2015, with 16.5% and 0~~2015. Time serie at Kharikhola station contains 34% ~~data gaps, respectively~~ of missing data in 2014–2015, corresponding to damages to the sensor (TABLE 3). Uncertainty on discharge is usually considered to account for less than 15% of discharge (Lang *et al.* 2006).

Recession times are computed on available recession periods using the lfstat R library (Koffler and Laaha 2013) with both the recession curves method (World Meteorological Organization 2008) and the base flow index method (Chapman 1999). We found recession times for Kharikhola and Tauche catchment of respectively around 70 days and around 67 days. Consequently, we consider that there is no interannual storage in either of the two catchments. This hypothesis can be modulated if a contribution of deep groundwater is considered (Andermann *et al.* 2011). Since these two catchments have null (Kharikhola) or neglectible (Tauche) glacier contribution, we hypothesized that the only entrance for water budgets in these catchments is total precipitation. In this study we used these two catchments as samples to assess generated precipitation fields against observed discharge at the local scale. The hydrological year is considered to start on 1 April, as decided by the Department of Hydrology and Meteorology of the Nepalese Government and generally considered (Nepal *et al.* 2014, Savéan *et al.* 2015).

Table 2. Overview of measurements at meteorological stations used in this study over the hydrological years 2014-2015 and 2015-2016. $\overline{T}$, $\overline{P}$ stand for, respectively, annual mean ~~temperatur~~ temperature and annual total precipitation. $\overline{T}$, $\overline{P}$ are computed on time series completed with either a weighted value at the closest station when available, or their respective interannual mean.

	2014-2015				2015-2016			
	Temperature		Precipitation		Temperature		Precipitation	
Station	$\overline{T}$	Gaps	$\overline{P}$	Gaps	$\overline{T}$	Gaps	$\overline{P}$	Gaps
	°C		mm		°C		mm	
KHA	13.96	0.1%	2453	34.5%	15.50	100%	1752	100%
MER	13.44	12.4%	3241	12.2%	14.83	100%	2278	100%
BAL	9.92	15.1%	3679	34.4%	10.48	0.0%	2628	0.0%
PHA	9.26	41.9%	1664	0.0%	9.16	0.0%	1226	0.0%
LUK	10.18	54.5%	2278	41.8%	10.19	40%	2278	0.2%
PAR	7.98	20%	3592	19.8%	7.84	100%	2540	100%
TCM	7.07	21.1%	3592	20.8%	6.90	100%	2628	100%
NAM	5.09	19.9%	964	0.1%	5.17	57.9%	788	0.1%
PAN	3.81	0.2%	876	0.0%	4.20	0.0%	526	0.0%
PHE	0.80	61%	701	0.0%	0.84	8.6%	526	0.0%
PYR	-2.71	18.6%	701	0.0%	-2.30	9.3%	438	0.0%

3. Spatialization methods for temperature and precipitation

3.1. *Temperature*

In mountainous areas, temperature and altitude generally correlate well linearly, considering a large time scale (Valéry *et al.* 2010, Gottardi *et al.* 2012).

Table 3. Overview of measurements at hydrological stations used in this study over the hydrological years 2014-2015 and 2015-2016. $\overline{Q}$ stands for annual discharge. $\overline{Q}$ for the Kharikhola station in 2014-2015 is completed with the interannual mean.

Station	2014-2015		2015-2016	
	$\overline{Q}$	Gaps	$\overline{Q}$	Gaps
	mm		mm	
Kharikhola	2341	34.0%	1746	0.0%
Pangboche	416	0.0%	499	0.0%

In the majority of studies based on field observations, air temperature values are extrapolated using the inverse distance weighting method (IDW) ~~(Andermann *et al.* 2012, Immerzeel *et al.* 2012, Nepal *et al.* 2014)~~(Andermann *et al.* 2012, Immerzeel *et* An altitude lapse rate θ (in $°C.km^{-1}$) is also used to take altitude into account for hourly temperature computation at any point M of the mesh extrapolated by IDW (EQUATION 1).

$$T(M) = \frac{\sum_{S_i} d^{-1}(M, S_i).(T(S_i) + \theta.(z_m - z_i))}{\sum_{S_i} d^{-1}(M, S_i)} \tag{1}$$

where T is the hourly temperature, S_i the ith station of the observation network, z_i the altitude of station S_i, z_M altitude of grid point M and d^{-1} is the inverse of distance in latitude and longitude.

In the Himalayas, seasonal (Nepal *et al.* 2014, Ragettli *et al.* 2015) or constant (Pokhrel *et al.* 2014) altitudinal lapse rates (LR) are used for temperature. FIGURE 2 presents seasonal LR computed from temperature time series at the 10 stations described in section 2.1. The linearity is particularly satisfying for both seasons, even if stations follow differently oriented transects (W-E or N-S orientation). Computed LR for both seasons are very close to values proposed by Immerzeel *et al.* (2014), Heynen *et al.* (2016) (Langtang catchment, 585 km^2, elevation ranging from 1406 m.a.s.l. to 7234 m.a.s.l.) and Salerno *et al.* (2015) (Koshi basin, 58100km^2, from 77 m.a.s.l. to 8848 m.a.s.l.). Consequently, these values for seasonal LR will be used in this study. Uncertainties associated with temperature interpolation will therefore be neglected, because they have minor impact on modelling compared to uncertainties on precipitation.

3.2. *Precipitation*

3.2.1. *Model of orographic precipitation*

The complexity of precipitation spatialization methods has beend commented by Barros and Lettenmaier (1993). When orographic effects are not well understood, complex approaches do not necessarily reproduce local measurements efficiently (Bénichou and Le Breton 1987, Frei and Schär 1998, Daly *et al.* 2002). In the Central Himalayas, various hydrologic and glaciological studies are based on observation networks to produce a precipitation grid. ~~They use either observed altitude lapse rates, e.g. , in the Langtang range, (Immerzeel *et al.* 2012, Ragettli *et al.* 2015) and~~in

6
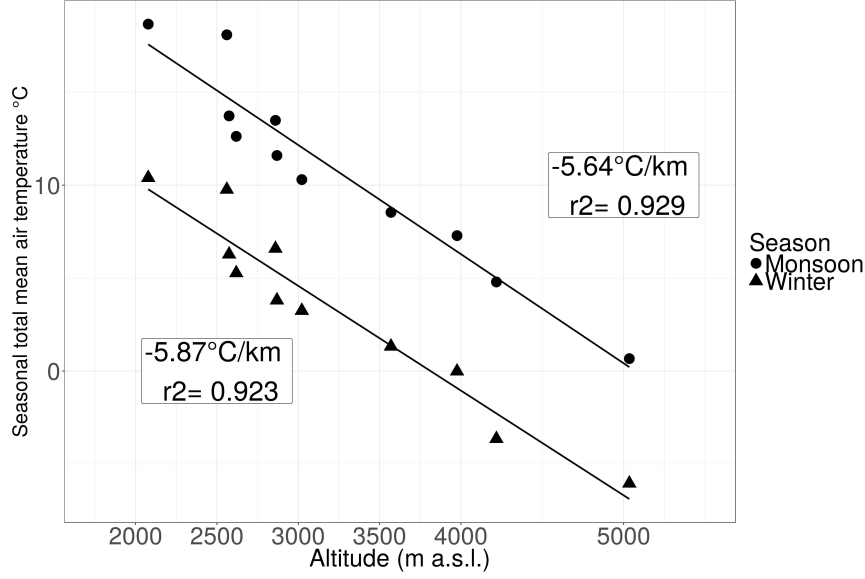
Figure 2. Linear regression for measured seasonal temperatures for the winter and monsoon seasons. Points (circles or triangles) are the seasonal means at each monitored station. Altitude lapse rates are displayed for each season in $^{\circ}C.km^{-1}$.

However, few studies provide precipitation fields at the hourly time scale (Ragettli *et al.* 2015, Heynen *et al.* 2016) and precipitation fields at spatial scales lower than 1 km are always obtained using altitude linear lapse rates (Immerzeel *et al.* 2012, Nepal *et al.* 2014, Pokhrel *et al.* 2014). However, the ~~Dudh Koshi River basin, (Nepal *et al.* 2014), or geostatistical methods (Gonga-Saholiariliva *et al.* 2016) (Koshi catchment). Nevertheless, the~~ considered lapse rates are constant in time and/or uniform in space. The spatial and temporal variability of the precipitation is then not represented in these studies. Moreover, the geostatistical cokriging method has been applied by Gonga-Saholiariliva *et al.* (2016) for monsoon precipitation interpolation over the Koshi catchment. However, the provided precipitation fields overally underestimate the observations, and this method is shown not to be adequate for the interpolation of solid precipitation. The IDW method is a simple, widely used method to spatialize precipitation in mountainous areas (Valéry *et al.* 2010, Gottardi *et al.* 2012, Duethmann *et al.* 2013, Nepal *et al.* 2014). In the French Alps, Valéry *et al.* (2010) combine the IDW method with a multiplicative altitudinal factor. Precipitation at any point M of the mesh extrapolated by the IDW is given by EQUATION 2.

$$P(M) = \frac{\displaystyle\sum_{S_i} d^{-1}(M, S_i).(P(S_i).exp(\beta(z_M - z_i)))}{\displaystyle\sum_{S_i} d^{-1}(M, S_i)} \tag{2}$$

In EQUATION 2, the altitude effect is represented through the introduction of the altitudinal factor β, defined by Valéry *et al.* (2010) as the slope of the linear regression between the altitude of stations (in m.a.s.l.) and the logarithm of seasonal volume of total precipitation expressed in millimeters. This method presents the advantage of

7

using an altitudinal factor which can vary in time and space. The spatial and temporal variability of the precipitation is therefore represented in this method. Moreover, the effect of altitude is independently studied and the controlling parameters have physical meaning.

3.2.2. Observed relation between altitude and seasonal precipitation

Several studies based on observations (Dhar and Rakhecha 1981, Barros *et al.* 2000, Bookhagen and Burbank 2006, Immerzeel *et al.* 2014, Salerno *et al.* 2015), or theoretical approaches (Burns 1953, Alpert 1986) observed that precipitation in the Himalayan range generally presents a multimodal distribution along elevation. Precipitation is considered to increase with altitude until a first altitudinal threshold located between 1800 m and 2500 m, depending on the study, and to decrease above ~~2500m~~2500 m. Moreover, the linear correlation of precipitation with altitude is reported to be weak for measurements above 4000 m (Salerno *et al.* 2015). The descreasing of precipitation with altitude ~~are~~ is characterized through various fonctions (Dhar and Rakhecha 1981, Bookhagen and Burbank 2006, Salerno *et al.* 2015). Nevertheless, the hypothesis of linearity of precipitation (P) with altitude (z) is often made, with a constant (Nepal *et al.* 2014) or time-dependent lapse rate (Immerzeel *et al.* 2014). Gottardi *et al.* (2012) noted that, in mountainous areas, the hypothesis of a linear relation between P and z is only acceptable over a small spatial extension and for homogeneous weather types. Consequently, we considered altitude lapse rates for precipitation at the seasonal time scale, and we analyzed the spatial variability of the relation between P and z.

For this purpose, we chose to regroup the stations into three groups (see FIGURE 1): 1) stations with elevation ranging from 2078 m to 3022 m, following a west-east transect (Group 1) ; 2) stations with elevation ranging from 2619 m to 3570 m following a south-west transect (Group 2); and 3) stations with elevation above 3970 m (Group 3). FIGURE 3 shows that 1) for Group 1, observed seasonal volumes of precipitation increase globally with altitude at a rate lower than $0.1 km^{-1}$; 2) for Group 2, seasonal volumes decrease at a rate around $-0.3 km^{-1}$; 3) for Group 3, seasonal volumes decrease at a rate lower than $0.2 km^{-1}$, with a poor linear trend.

The overlapping of altitude ranges between Group 1 and Group 2 highlights that the relation between precipitation and altitude strongly depends on terrain orientation. The difference in seasonal volumes at the BAL (2575 m a.s.l., 3471 mm/year) and MER stations (2561 m a.s.l., 2245 mm/year) (GROUP 1) also result from site effects on precipitation. In summary, β values inferred from local observations mainly express local variability and are not sufficient to establish any explicit relation between precipitation and altitude at the catchment scale. However, for operational purposes, the β factor can be simplified as a multi-modal function of altitude within the Dudh Koshi catchment. ~~Optimum values that optimally fit local variability were then investigated through a sensitivity and uncertainty analysis.~~ The β factor is represented as a piecewise linear function of altitude using two ~~altitudinal~~ altitude thresholds z_1 and z_2 and three altitude lapse rates β_1, β_2 and β_3 (EQUATION 3).

8
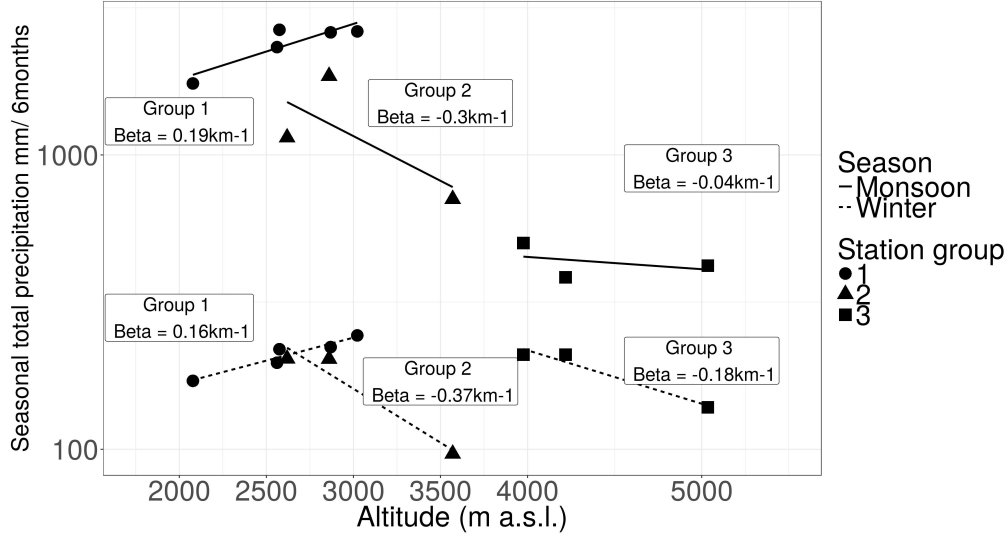
Figure 3. Piecewise relation between altitude and the logarithm of observed seasonal volumes of total precipitation, separated by season and station group. Seasonal values for β (km^{-1}) are computed from observed precipitation for each of the three station groups.

$$
\beta(z) = \left\{ \begin{array}{lll} \beta_1 > 0 & \text{if} & z \leq z_1 \\ \beta_2 < 0 & \text{if} & z_1 < z \leq z_2 \\ \beta_3 \sim 0 & \text{if} & z > z_2 \end{array} \right. \tag{3}
$$

Since no deterministic value can be ensured for the five parameters controlling the shape of EQUATION 3, an ensemble approach was applied (see Section 4) to estimate parameter sets at the scale of the entire Dudh Koshi River basin that are optimally suitable for both Tauche and Kharikhola catchments.

4. Sensitivity and uncertainties analysis method

4.1. *Overall strategy*

Saltelli *et al.* (2006) distinguishes sensitivity analysis (SA), which does not provide a measurement of error, and uncertainties analysis (UA), which computes a likelihood function according to reference data. SA is run before UA as a diagnostic tool, in particular to reduce variation intervals for parameters and therefore save computation time.

The algorithm chosen for SA was the Regional Sensitivity Analysis (RSA) (Spear and Hornberger 1980) method. The RSA method is based on the separation of the parameter space into (at least) two groups: behavioral or nonbehavioral parameter sets. A behavioral parameter set is a set that respects conditions (maximum or minimum thresholds) on the output of the orographic precipitation model. Thresholds will be defined for solid and total precipitation in the Results section. The analysis is performed using the R version of the SAFE(R) toolbox, developed by Pianosi *et al.* (2015).

SA and UA are set up as follows (Beven 2010):

9

(1) First, the parameter space is sampled, according to a given sampling distribution. For each parameter set, hourly precipitation fields are computed at the 1-km resolution using EQUATION 2 for both the Tauche and Kharikhola catchments. Since physical processes condition the relation between altitude and precipitation strongly differ between the two seasons, we chose to distinguish altitude correction for the winter and monsoon seasons. Behavioral parameter sets were then selected for each of the two seasons.

(2) Then, for each behavioral precipitation field, the ISBA surface scheme, described in the next section, was run separately on Kharikhola and Tauche catchments. The objective function was computed as the difference between simulated and observed annual discharge at the outlet of each catchment. Parameter sets that lead to acceptable discharge regarding observed discharge for the two catchments are finally selected.

4.2.   Hydrological modeling at the local scale

4.2.1.   The ISBA surface scheme

We considered that there was no interannual storage in either of the two subcatchments studied, i.e., the variation of the groundwater content was considered null from one hydrological year to the other. Consequently, annual simulated discharges were computed as the sum over all grid cells and all time steps, of simulated surface flow and simulated subsurface flow. The question of calibration of flow routing in the catchment was thus avoided.

The ISBA surface scheme (Noilhan and Planton 1989, Noilhan and Mahfouf 1996) simulates interactions between the soil, vegetation and the atmosphere on a ~~sub-hourly~~ subhourly time step (SVAT model). The multi-layer version of ISBA (ISBA-DIF) uses a diffusive approach (Boone *et al.* 2000, Decharme *et al.* 2011): surface and soil water fluxes are propagated from the surface through the soil column. Transport equations for mass and energy are solving using a multilayer vertical discretization of the soil. The explicit snow scheme in ISBA (ISBA-ES) Boone and Etchevers (2001) uses a three-layer vertical discretization of snow pack and provides a mass and energy balance for each layer (Boone and Etchevers 2001). Snow-melt and snow sublimation are taken into account in balance equations. The separation between runoff over saturated areas (Dunne runoff), infiltration excess runoff (Horton runoff) and infiltration is controled by the Variable Infiltration Capacity Scheme (VIC) (Dümenil and Todini 1992).

The precipitation phase was estimated depending on hourly air temperature readings. Mixed phases occurred for temperatures between 0°C and 2°C, following a linear relation. Other input variables required for ISBA (atmospheric pressure, relative humidity, wind speed, short- and long-wave radiations) ~~are~~ were interpolated from measurements at Pyramid station as functions of altitude, using the method proposed by Cosgrove *et al.* (2003). Short wave radiation and wind speed are not spatially interpolated and are considered to be equals to the measurements at Pyramid station for the two catchments.

4.2.2. Parametrization of surfaces

Several products provide parameter sets for physical properties of surfaces at the global scale (Hagemann 2002, Masson *et al.* 2003, Arino *et al.* 2012). However, these products are not accurate enough at the resolution required for this study. The most recent analysis (Bharati *et al.* 2014, Ragettli *et al.* 2015) exclusively used knowledge garnered from the literature. To detail the approach, in this study the parametrization was based on in situ measurements. A classification into nine classes of soil/vegetation entities was defined based on Sentinel2 images at a 10-m resolution (Drusch *et al.* 2012), using a supervised classification tool of the QGIS Semi-Automatic Classification Plugin (Congedo 2015).

In and around the two cathchments, 24 reference sites were sampled during field missions. Data collection included soil texture, soil depth, root depth, determined by augering to a maximum depth of 1.2m. Vegetation height, structure and dominant plant species were also determined. The results were classified into nine surface types. The nine classes and their respective fractions in Kharikhola and Tauche catchments are presented TABLE 4.

Analysis of soil samples showed that soils were mostly sandy ($\sim$ 70%), with a small proportion of clay ($\sim$ 1%). Soil depths varied from very thin ($\sim$ 30 cm) at high altitudes to 1.2 m for flat cultivated areas. Forest areas were separated into three classes: dry forests were characterized by high slopes and shallow soils; wet forests presented deep silty soils (1 m), with high trees (7 m). Intermediate forests had moderate slopes and relatively deep, sandy soils. Crop areas presented different soil depths depending on their average slope. In addition, values for unmeasured variables (LAI, soil and vegetation albedos, surface emissivity, surface roughness) were taken from the ~~ECOCLIMAP~~ ECOCLIMAP1 classification (Masson *et al.* 2003) for ecosystems representative of the study area. ~~ECOCLIMAP~~ ECOCLIMAP1 provides the annual cycle of dynamic vegetation variables, based both on a surface properties classification (Hagemann 2002) and on a global climate map (Koeppe and De Long 1958). The ECOCLIMAP2 product (Faroux *et al.* 2013) is derived from ECOCLIMAP1 and provides enhanced descriptions of surfaces. However, ECOCLIMAP2 is only available over Europe and therefore is not used in this study.

5. Results and discussion

5.1. *Regional sensitivity analysis*

The parameter space was sampled using the ~~All at a time~~ *All at a time* (AAT) sampling algorithm from the SAFE(R) toolbox (Pianosi *et al.* 2015). Since no particular information was available on prior distribution and interaction for the five parameters, uniform distributions were considered. The ~~initial ranges for~~ size of parameter samples was chosen according to Sarrazin *et al.* (2016) (TABLE 5). The optimization method is highly sensitive to the choice of inital values for the β_1, β_2 ~~and~~, β_3 ~~parameters were defined based on the lapse rates computed at the seasonal time scale from observations. Ranges for altitudinal~~, z1 and z2 parameters. Several attempts have been done and the choices presented TABLE 6 are justified by the following arguments:
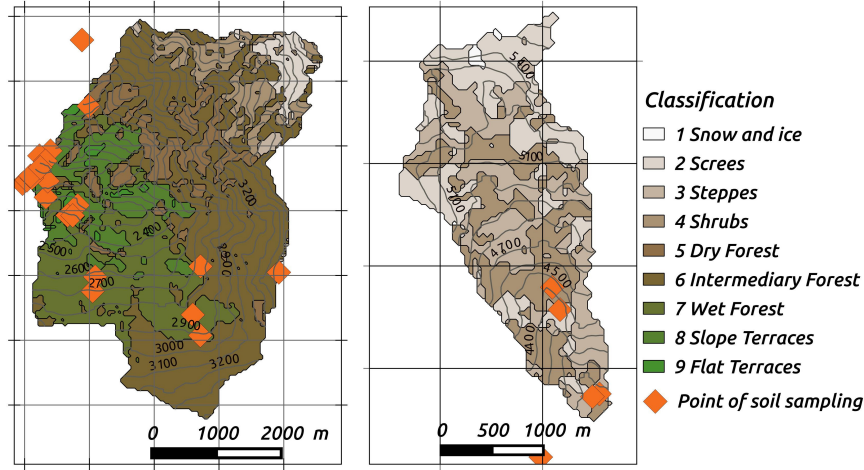
Figure 4. Classification of surfaces defined for the two Kharikhola and Tauche subcatchments, established using the supervised classification tool of the QGIS Semi-Automatic Classification Plugin (Congedo 2015), based on Sentinel2 images at a 10-m resolution (Drusch *et al.* 2012). In situ sample points were used to describe the soil and vegetation characteristics of each class.

Table 4. Soil and vegetation characteristics of the nine classes defined in Kharikhola and Tauche catchments, respectively. % KK and % Tauche are the fraction of each class on Kharikhola and Tauche catchments. Sand and clay fractions (% Sand and % Clay, respectively), soil depth (SD), root depth (RD) and tree height (TH) are defined based on in situ measurements. The dynamic variables (e.g. the fraction of vegetation and Leaf Area Index) were found in the ~~ECOCLIMAP~~ ECOCLIMAP1 classification (Masson *et al.* 2003) for representative ecosystems.

ID	Class	% KK	% Tauche	% Sand	% Clay	TH m	SD m	RD m	~~Ecoclimap~~ ECOCLIMAP1 Cover
1	Snow and ice	-	0.7%	0.00	0.00	0.0	0.00	0.00	6
2	Screes	3.1%	31.2%	0.00	0.00	0.0	0.00	0.00	5
3	Steppe	0.6%	33.7%	81.41	1.70	0.0	0.10	0.10	123
4	Shrubs	7.4%	34.4%	70.60	1.55	0.0	0.35	0.27	86
5	Dry Forest	9.7%	-	72.86	1.00	12.0	0.20	0.20	27
6	Intermediary Forest	45.7%	-	84.97	1.01	27.5	0.42	0.40	27
7	Wet Forest	20.6%	-	70.12	1.00	6.8	1.04	0.50	27
8	Slope terraces	11.2%	-	70.89	1.38	5.6	0.56	0.26	171
9	Flat terraces	1.4%	-	67.01	1.69	2.5	1.267	0.20	171

- Minimum and maximum values for the altitude thresholds z1 and z2 ~~were deduced from other studies (Bookhagen and Burbank 2006, Nepal 2012, Savéan 2014). The initial ranges are given in TABLE 6. The size of parameter samples was chosen according to Sarrazin *et al.* (2016) (TABLE 5).~~ are chosen accordingly to both litterature review (Barros *et al.* 2000, Anders *et al.* 2006, Bookhagen and Burbank 2006, Shrestha *et al.* 2012, Nepal observations. The first inquired altitudinal threshold is described in litterature between 2000 m and 3000 m and the second threshold is described above 4000 m. These intervals have been enlarged to also test related values.

- Maximum (resp. minimum) value for β_1 (resp. β_2) are chosen about 10 times larger than the value computed based on observation. Considering the definition of the beta coefficient, a value greater than 2 km^{-1} (resp. lower than -2 km^{-1}) would lead to a multiplication of precipitation by 1.22 (resp. by 0.82) within 100

12

m. When applied to the precipitation oberved at stations, this would lead to inconsistent precipitation when increasing altitude by 100 m.

- The β_3 coefficient has to be negative because a positive value would lead to unrealistic values at high altitudes. Moreover, the minimum value is chosen to be significantly smaller than the value computed for β_3 based on the observations, but also to remain higer than the value computed for β_2 based on the observations.

A behavioral parameter set is a set that leads to an annual amount of total precipitation for both catchments comprised between a minimum and a maximum value. A parameter sets that does not meet these conditions is considered as nonbehavioral. Maximum and minimum conditions on annual total precipitation for a set to be behavioral were chosen according to annual observed discharge for each of the two catchments. The mean observed discharge for the recorded period was 2043 mm/year at the Kharikhola station and 457 mm/year at the Tauche station. Annual total precipitation was expected to be greater than the measured annual discharge and lower than annual discharge plus 70%. These thresholds take into account both the uncertainty on measured discharges and actual evapotranspiration. Based ~~no a~~ on values proposed in the literature, evapotranspiration is assumed to represent less than 50% of observed discharge, for both catchments. The minimum and maximum thresholds for both catchments are summarized TABLE 7.

The method's convergence (i.e., the stability of the result when the sample size grows) was graphically assessed. The results converged for sample sizes from 1000 samples. FIGURE 5 shows the cumulative density function (CDF) for behavioral and nonbehavioral parameter sets for the monsoon and winter seasons. Of the 2000 parameter sets sampled, 712 sets verified the chosen minimum and maximum conditions for annual total precipitation and snowfall (i.e., they were behavioral). The sensitivity of the output to each parameter was evaluated by the maximum vertical distance (MVD) between CDF for both behavioral and nonbehavioral parameter sets. Annual total precipitation appeared to be less sensitive to parameters controlling winter precipitation than to parameters controlling monsoon precipitation. This result can be explained by the fact that winter precipitation was less than monsoon precipitation. However, since the applied sampling method does not take into account the existing interaction between the five parameters, further analysis for parameter ranking was not significant.

The method was necessarily sensitive to the prior hypothesis presented TABLE 5. In particular, the conditions for a set to be behavioral have a significant impact on the distribution of the behavioral sets. On the contrary, increasing the sample size does not affect the output distribution, since minimum size for convergence is reached.

Table 5. The algorithm selected, sample size and prior distribution for sampling the parameter space using the SAFE(R) toolbox (Pianosi *et al.* 2015).

Sample size	2000
Nb. of model evaluation	2000
Sampling algorithm	All-at-a-Time
Sampling method	Latin Hypercube
Prior distributions	Uniforms

13

Table 6. Initial ranges considered for the five shape parameters of the altitudinal factor: z1, z2 β_1, β_2 and β_3. Ranges are defined based on measurements at stations and on values founded in the literature.

	Minimum	Maximum	
z1	1900	3500	m. a.s.l.
z2	3500	6500	m. a.s.l.
β_1	0.00	2.00	km^{-1}
β_2	-2.00	0.00	km^{-1}
β_3	-0.30	0.00	km^{-1}

Table 7. Conditions over total precipitation on the Kharikhola and Tauche catchments for a parameter set to be behavioral. Annual total precipitation was expected to be greater than the measured annual discharge plus 20% and lower than annual discharge plus 50%.

	Minimum	Maximum	
Kharikhola	2043	3473	mm/year
Tauche	457	777	mm/year
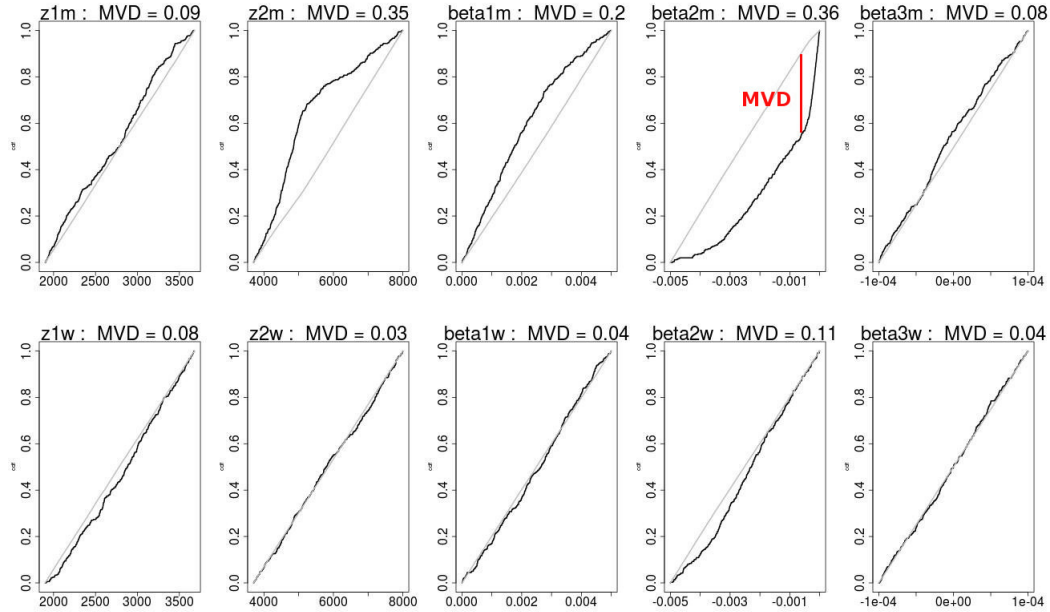
Figure 5. Cumulative density function of behavioral and non-behavioral output for each parameter for the two seasons. Black lines are cumulative distributions of behavioral parameter sets, and grey lines are cumulative distributions of non-behavioral sets. Parameters with indication w (respectively, m) stand for winter values (respectively, monsoon values). The greater the maximum vertical distance (MVD), the more influential the parameter was. MVD is drawn as an example for parameter beta2m.

5.2. *Uncertainties analysis*

5.2.1. *Annual simulated water budgets*

The precipitation fields generated using each behavioral parameter set were used as input data within the ISBA surface scheme. The simulation over the Tauche and Kharikhola catchments were run separately over the 2013-01-01/2016-03-31 period, at

the hourly time scale. The 2013–2014 hydrological year was used as a spin-up period
and the results were observed for 2014–2015 and 2015–2016 hydrological years. To
overcome the issue of calibrating a flow-routing module, the simulated discharge were
aggregated at the annual time scale and compared to annual observed discharge at
the outlet ($\overline{Q}_{obs}$).

FIGURE 6 presents boxplots obtained for the 712 behavioral parameter sets for the
terms of the annual water budget, i.e., liquid and solid precipitation, discharge and
evapotranspiration. The dotted line represents $\overline{Q}_{obs}$ for each catchment. The mean
annual volumes of simulated variables were also computed for each parameter set in
2014–2015 and 2015–2016, and the intervals of uncertainty associated with simulated
annual volumes are provided. This method highlights the propagation of uncertainties
associated with the representation of orographic effects toward simulated terms of
annual water budgets.

TABLE 8 presents the mean value, standard deviation and relative standard
deviation for all of the ISBA simulated variables for the Kharikhola and Tauche
catchments, for 2014–2015 and 2015–2016. The annual actual evapotranspiration
accounted for 26% of annual total precipitation for Kharikhola and 34% for Tauche.
In comparison, evapotranspiration was estimated at about 20%, 14% and 53% of total
annual precipitation, respectively, by (Andermann *et al.* 2012),(Nepal *et al.* 2014)
and (Savéan *et al.* 2015) over the entire Dudh Koshi basin and (Ragettli *et al.* 2015)
estimated it at 36.2% of annual total precipitation for the upper part of the Langtang
basin.

Annual snow fall volume for Kharikhola was a neglectible fraction of annual
total precipitation ($\sim$1%) and it was around 44% for Tauche. Annual snowfall was
estimated at, respectively, 15.6% and 51.4% of annual total precipitation by (Savéan
et al. 2015) (entire Dudh Koshi river basin) and (Ragettli *et al.* 2015) (upper part of
the Langtang basin).

Moreover, this statistical approach shows that the only uncertainties associated with
representation of the orographic effect results in significant uncertainties on simulated
variables. These uncertainties account for up to 16% for annual total precipitation,
up to 25% for annual discharge and up to 8% for annual actual evapotranspiration.
Uncertainty on annual snowfall is quantified at 16% for high mountain catchment and
up to 32% for middle mountain catchment. These uncertainty intervals are essentially
conditioned by model structure and parametrization, and these results point out that
simulated water budgets provided by modelling studies must necessarily be associated
with error intervals.

### 5.2.2. *Toward optimizing parameter sets with bias on annual discharge*

Going further into the simulation results, the hydrological cycle was inverted, in order
to use observed discharge to optimize the relation between precipitation and altitude,
as presented for mountainous areas by Valéry *et al.* (2009). Precipitation fields were
then constrained at the local scale according to simulated discharges. Annual bias
on discharge were computed for each catchment as the absolute value of the ratio
between the observed and simulated annual discharges minus 1. FIGURE 7 presents
the scatter plot of the distributions of bias on annual discharge for the Kharikhola
and Tauche catchments. The Pareto optimums minimizing bias on annual discharge

Table 8. Mean values (X), standard deviation ($\overline{X}$) and relative standard deviation ($\sigma/\overline{X}$) for total precipitation (PTOT), snowfall (SNOWF), discharge (RUNOFF) and actual evapotranspiration (EVAP) simulated with ISBA for the Kharikhola catchment or Tauche catchment: the mean for 2014–2015 and 2015–2016.

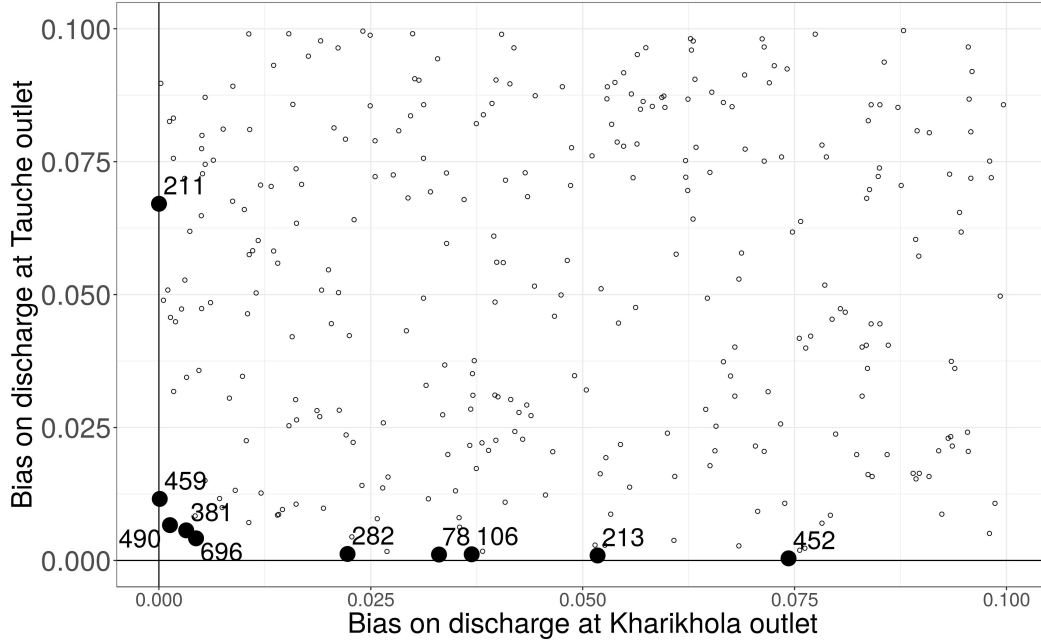| | Kharikhola catchment | | | | | | Tauche catchment | | | | | |
	2014-2015			2015-2016			2014-2015			2015-2016		
	$\overline{X}$	σ	$\sigma/\overline{X}$	$\overline{X}$	σ	$\sigma/\overline{X}$	$\overline{X}$	σ	$\sigma/\overline{X}$	$\overline{X}$	σ	$\sigma/\overline{X}$
	mm	mm	-	mm	mm	-	mm	mm	-	mm	mm	-
EVAP	604	17	3%	664	16	2%	213	16	8%	219	15	7%
PTOT	2868	295	10%	2069	207	10%	766	110	14%	525	82	16%
RUNOFF	2279	293	13%	1421	203	14%	517	128	25%	459	85	19%
SNOWF	32	8	25%	22	7	32%	364	56	15%	205	35	17%
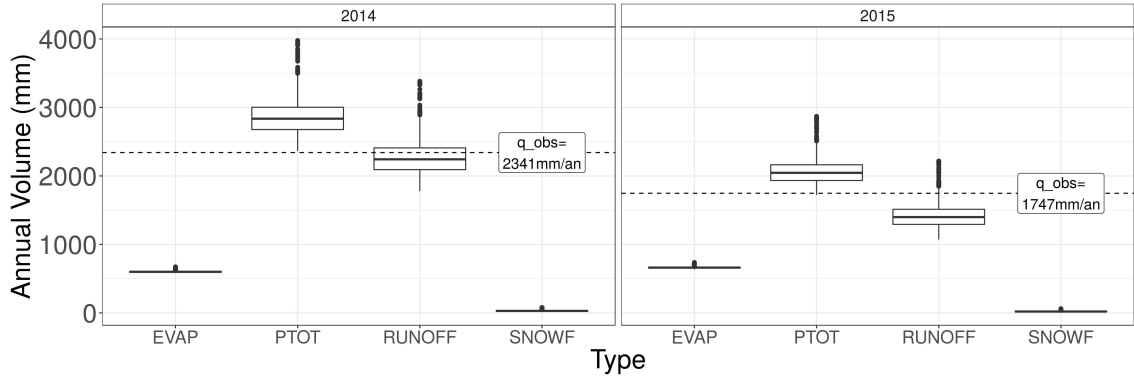
(a) For Kharikhola catchment.
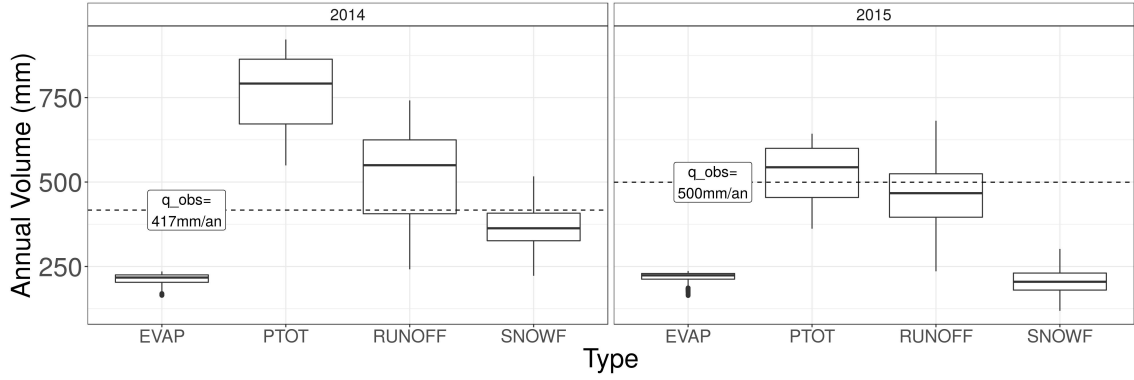
(b) For Tauche catchment.

Figure 6. Boxplots for distribution of annual volumes of the terms of the water budget: Discharge (RUNOFF), solid and total precipitation (SNOWF and PTOT) and evapotranspiration (EVAP) for 2014–2015, for the Kharikhola and Tauche catchments.

for both catchments were computed using the R rPref package (Roocks and Roocks 2016). For exemple, the ten first Pareto optimums were selected among the 712 behavioral parameter sets considered. The values of parameters for the winter and monsoon seasons for the ten first optimum sets are summarized in TABLE 9. For the ten parameter sets selected, the altitudinal threshold z1 was located between 2010 m.a.s.l. and 3470 m.a.s.l. during the monsoon season and between 2287 m.a.s.l. and 3488 m.a.s.l. during winter. The second altitudinal threshold z2 was located between 3709 m.a.s.l.

and 6167 m.a.s.l. during monsoon and between 3734 m.a.s.l. and 6466 m.a.s.l. during
winter. Altitudes found for z1 were globally higher than altitudes proposed in the lit-
erature for the second mode of precipitation (between 1800 m.a.s.l. and 2400 m.a.s.l.,
as described in section 3.2.2). Since these values were calibrated at the local scale, ac-
cording to ground-based measurements, they can be considered to accurately represent
the local variability encountered in the Tauche and Kharikhola catchments. Moreover,
values for an altitudinal threshold of precipitation located above 4000 m.a.s.l. were
proposed.

Figure 7. Scatter plot of bias on mean annual discharges for the Kharikhola and Tauche catchments for 2014–2015. Darker dots are parameter sets that provide the ten first Pareto optimums according to both criteria: bias for discharges on the Kharikhola and Tauche catchments. Optimal value for bias is 0. Graphical window is limited.

Table 9. Values of parameters for the winter and monsoon seasons for the ten first Pareto optimum sets. The Pareto optimums minimize bias on annual discharge for both catchments.

Sample $n°$	78	106	211	213	282	381	452	459	490	696	
z1m	3470	3066	3286	2010	2971	2946	3337	2333	2064	2253	m.a.s.l.
z2m	3709	4938	6101	4379	4813	5596	5681	3915	6167	5978	m.a.s.l.
beta1m	0.032	0.028	0.455	1.772	1.089	1.755	0.787	0.73	0.135	0.003	km^{-1}
beta2m	-1.382	-0.48	-0.556	-0.143	-0.169	-0.397	-0.516	-1.394	-0.587	-0.341	km^{-1}
beta3m	-0.283	-0.229	-0.059	-0.207	-0.298	-0.037	-0.003	-0.25	-0.033	-0.111	km^{-1}
z1w	3113	2727	2287	2895	3236	2623	2446	3488	2554	2639	m.a.s.l.
z2w	4943	4716	3871	6466	5657	3734	4336	5163	4732	5155	m.a.s.l.
beta1w	1.917	0.288	0.869	1.533	1.658	0.293	0.115	1.729	1.256	0.348	km^{-1}
beta2w	-1.83	-1.096	-1.588	-1.791	-0.804	-0.455	-1.568	-1.457	-1.612	-0.508	km^{-1}
beta3w	-0.191	-0.2	-0.255	-0.244	-0.068	-0.165	-0.294	-0.011	-0.039	-0.037	km^{-1}
bias Khari.	0.033	0.037	0	0.052	0.022	0.003	0.074	0	0.001	0.004	
bias Tauche	0.001	0.001	0.067	0.001	0.001	0.006	0	0.012	0.007	0.004	

17

488 *5.2.3. Ensemble of hourly precipitation fields on the Dudh Koshi River basin*

489 Observed precipitation at measuring stations were then interpolated at the hourly time
490 scale over the Dudh Koshi River basin at the 1-km spatial resolution. The method
491 given by EQUATION 2 is applied, using shape parameters for the altitudinal factor
492 selected TABLE 9. The average annual volumes of computed total precipitation ranged
493 between 1365 mm and 1652 mm, and annual snowfall volumes ranged between 89 mm
494 and 126 mm, in average over the 2014–2015 and 2015–2016 hydrological years. These
495 values are consistent with other products available for the area. In particular, Savéan
496 (2014) showed that the APHRODITE (Yatagai *et al.* 2012) product underestimates
497 total precipitation over the Dudh Koshi River basin, with annual total precipitation of
498 1311 mm for the interannual average between 2001 and 2007, and Nepal *et al.* (2014)
499 proposed a mean annual total precipitation for the Dudh Koshi basin of 2114 mm
500 over the 1986–1997 period. The ERA-Interim reanalysis (25-km resolution) provided a
501 mean annual precipitation of 1743 mm over the 2000–2013 period. Different relations
502 between altitude and annual precipitation are then represented. The higher (lower)
503 values are the positive (negative) rates, the sharpest are the spatial variations of annual
504 precipitation. This has to be discussed considering the physical properties of convection
505 at such high altitudes.

506 ## 6. Conclusion

507 The main objective of this paper was to provide a representation of the effect of alti-
508 tude on precipitation that represent spatial and temporal variability of precipitation
509 in the Everest region. A weighted inverse distance method coupled with a multiplica-
510 tive altitudinal factor was applied to spatially extrapolate measured precipitation
511 to produce precipitation fields over the Dudh Koshi basin. The altitudinal factor
512 for the Dudh Koshi basin is shown to acceptably fit a piecewise linear function of
513 altitude, with significant seasonal variations. A sensitivity analysis was run to reduce
514 the variation interval for parameters controlling the shape of the altitudinal factor.
515 An uncertainty analysis was subsequently run to evaluated ensemble of simulated
516 variables according to observed discharge for two small subcatchments of the Dudh
517 Koshi basin located in mid- and high-altitude mountain environments.
518
519 Non deterministic annual water budgets are provided for two small gauged
520 subcatchments located in high- and mid-altitude mountain environments. This work
521 shows that the only uncertainties associated with representation of the orographic ef-
522 fect account for about 16% for annual total precipitation and up to 25% for simulated
523 discharges. Annual evapotranspiration is shown to represent $26\% \pm 1\%$ of annual
524 total precipitation for the mid-altitude catchment and $34\% \pm 3\%$ for the high-altitude
525 catchment. Snow fall contribution is shown to be neglectible for the mid-altitude
526 catchment and it represents up to $44\% \pm 8\%$ of total precipitation for the high-altitude
527 catchment. These simulations at the local scale enhance current knowledge of the
528 spatial variability of hydro-climatic processes in high- and mid-altitude mountain
529 environments.
530
531 This work paves the way to produce hourly precipitation maps extrapolated from
532 ground-based measurements that are reliable at the local scale. However, additional
533 criteria would be needed to provide a single optimum parameter set for altitudinal

18

factor that would be suitable for the entire Dudh Koshi River basin. For exemple, snow cover areas simulated at a scale larger than the two catchments could be compared to available remote products (Behrangi *et al.* 2016). Independent measurements of precipitation could also be used to constrain the ensemble of precipitation fields.

Moreover, since observations are made over a very short duration and contain long periods with missing information, the results are limited to the 2014–2015 and 2015–2016 hydrological years and to the Dudh Koshi River basin. In addition, this study focuses only on one source of uncertainty in the measurement-spatialization-modeling chain, whereas sensitivity analysis should include all types of uncertainty (Beven 2015, Saltelli *et al.* 2006). A more complete method would include epistemic uncertainty on model parameters and aleatory uncertainty on input variables in the sensitivity analysis (Fuentes Andino *et al.* 2016).

References

Alpert, P., 1986. Mesoscale indexing of the distribution of orographic precipitation over high mountains. *Journal of climate and applied meteorology*, 25 (4), 532–545.

Andermann, C., *et al.*, 2012. Impact of transient groundwater storage on the discharge of himalayan rivers. *Nature Geoscience*, 5 (2), 127–132.

Andermann, C., Bonnet, S., and Gloaguen, R., 2011. Evaluation of precipitation data sets along the himalayan front. *Geochemistry, Geophysics, Geosystems*, 12 (7).

19

Anders, A.M., *et al.*, 2006. Spatial patterns of precipitation and topography in the himalaya. *Geological Society of America Special Papers*, 398, 39–53.

Arino, O., *et al.*, 2012. Global land cover map for 2009 (globcover 2009).

Barros, A.P. and Lettenmaier, D.P., 1993. Dynamic modeling of the spatial distribution of precipitation in remote mountainous areas. *Monthly weather review*, 121 (4), 1195–1214.

Barros, A., *et al.*, 2000. A study of the 1999 monsoon rainfall in a mountainous region in central nepal using trmm products and rain gauge observations. *Geophysical Research Letters*, 27 (22), 3683–3686.

Barros, A., *et al.*, 2004. Probing orographic controls in the himalayas during the monsoon using satellite imagery. *Natural Hazards and Earth System Science*, 4 (1), 29–51.

Behrangi, A., *et al.*, 2016. Using grace to constrain precipitation amount over cold mountainous basins. *Geophysical Research Letters*.

Bénichou, P. and Le Breton, O., 1987. AURELHY : une méthode d'analyse utilisant le relief pour les besoins de l'hydrométéorologie. *In*: *Deuxièmes journées hydrologiques de l'ORSTOM à Montpellier*. Colloques et Séminaires. ORSTOM, 299–304. Available from: http://www.documentation.ird.fr/hor/fdi:25973.

Beven, K., 2010. *Environmental modelling: An uncertain future?* CRC Press.

Beven, K., 2015. Facets of uncertainty: epistemic uncertainty, non-stationarity, likelihood, hypothesis testing, and communication. *Hydrological Sciences Journal*, (just-accepted).

Bharati, L., *et al.*, 2014. The Projected Impact of Climate Change on Water Availability and Development in the Koshi Basin, Nepal. *Mountain Research and Development*, 34 (2), 118–130. Available from: http://www.bioone.org/doi/abs/10.1659/MRD-JOURNAL-D-13-00096.1.

Bharati, L., *et al.*, 2016. Past and future variability in the hydrological regime of the koshi basin, nepal. *Hydrological Sciences Journal*, 61 (1), 79–93.

Bookhagen, B. and Burbank, D.W., 2006. Topography, relief, and trmm-derived rainfall variations along the himalaya. *Geophysical Research Letters*, 33 (8). Available from: http://dx.doi.org/10.1029/2006GL026037.

Bookhagen, B. and Burbank, D.W., 2010. Toward a complete Himalayan hydrological budget: Spatiotemporal distribution of snowmelt and rainfall and their impact on river discharge. *Journal of geophysical research-Earth surface*, 115.

Boone, A., *et al.*, 2000. The influence of the inclusion of soil freezing on simulations by a soil-vegetation-atmosphere transfer scheme. *JOURNAL OF APPLIED METEOROLOGY*, 39 (9), 1544–1569.

Boone, A. and Etchevers, P., 2001. An intercomparison of three snow schemes of varying complexity coupled to the same land surface model: Local-scale evaluation at an alpine site. *Journal of Hydrometeorology*, 2 (4), 374–394. Available from: http://dx.doi.org/10.1175/1525-7541(2001)002¡0374:AIOTSS¿2.0.CO;2.

Burns, J.I., 1953. Small-scale topographic effects on precipitation distribution in san dimas experimental forest. *Eos, Transactions American Geophysical Union*, 34 (5), 761–768.

Chapman, T., 1999. A comparison of algorithms for stream flow recession and baseflow separation. *Hydrological Processes*, 13 (5), 701–714. Available from: http://dx.doi.org/10.1002/(SICI)1099-1085(19990415)13:5¡701::AID-HYP774¿3.0.CO;2-2.

Congedo, L., 2015. Semi-automatic classification plugin documentation. *Release*, 4 (0.1), 29.

Cosgrove, B., *et al.*, 2003. Real-time and retrospective forcing in the North American Land Data Assimilation System (NLDAS) project. *JOURNAL OF GEOPHYSICAL RESEARCH-ATMOSPHERES*, 108 (D22).

Daly, C., *et al.*, 2002. A knowledge-based approach to the statistical mapping of climate. *Climate research*, 22 (2), 99–113.

Decharme, B., *et al.*, 2011. Local evaluation of the Interaction between Soil Biosphere Atmosphere soil multilayer diffusion scheme using four pedotransfer functions. *JOURNAL OF GEOPHYSICAL RESEARCH-ATMOSPHERES*, 116.

Dhar, O. and Rakhecha, P., 1981. The effect of elevation on monsoon rainfall distribution in the central himalayas. *Monsoon Dynamics*, 253–260.

629 Drusch, M., *et al.*, 2012. Sentinel-2: Esa's optical high-resolution mission for gmes operational
630   services. *Remote Sensing of Environment*, 120, 25–36.

631 Duethmann, D., *et al.*, 2013. Evaluation of areal precipitation estimates based on downscaled
632   reanalysis and station data by hydrological modelling. *Hydrology and Earth System Sciences*,
633   17 (7), 2415–2434. Available from: http://www.hydrol-earth-syst-sci.net/17/2415/2013/.

634 Dümenil, L. and Todini, E., 1992. A rainfall-runoff scheme for use in the hamburg climate
635   model. *In*: *Advances in theoretical hydrology: a tribute to james dooge*. Elsevier Science
636   Publishers BV, 129–157.

637 Faroux, S., *et al.*, 2013. Ecoclimap-ii/europe: a twofold database of ecosystems and surface
638   parameters at 1 km resolution based on satellite information for use in land surface, mete-
639   orological and climate models. *Geoscientific Model Development*, 6 (2), 563–582.

640 Frei, C. and Schär, C., 1998. A precipitation climatology of the alps from high-resolution
641   rain-gauge observations. *International Journal of climatology*, 18 (8), 873–900.

642 Fuentes Andino, D., *et al.*, 2016. Event and model dependent rainfall adjustments to improve
643   discharge predictions. *Hydrological Sciences Journal*, (just-accepted).

644 Gonga-Saholiariliva, N., *et al.*, 2016. Geostatistical estimation of daily monsoon precipitation
645   at fine spatial scale: Koshi river basin. *Journal of Hydrologic Engineering*, 05016017.

646 Gottardi, F., *et al.*, 2012. Statistical reanalysis of precipitation fields based on ground network
647   data and weather patterns: Application over french mountains. *Journal of Hydrology*, 432,
648   154–167.

649 Hagemann, S., 2002. *An improved land surface parameter dataset for global and regional climate*
650   *models*. Max-Planck-Institut für Meteorologie.

651 Heynen, M., *et al.*, 2016. Air temperature variability in a high-elevation himalayan catchment.
652   *Annals of Glaciology*, 57 (71), 212–222.

653 Immerzeel, W.W., *et al.*, 2012. Hydrological response to climate change in a glacierized catch-
654   ment in the Himalayas. *Climatic change*, 110 (3-4), 721–736.

655 Immerzeel, W., *et al.*, 2014. The importance of observed gradients of air temperature and
656   precipitation for modeling runoff from a glacierized watershed in the nepalese himalayas.
657   *Water Resources Research*, 50 (3), 2212–2226.

658 Kansakar, S.R., *et al.*, 2004. Spatial pattern in the precipitation regime of nepal. *International*
659   *Journal of Climatology*, 24 (13), 1645–1659.

660 Koeppe, C.E. and De Long, G., 1958. Weather and climate.

661 Koffler, D. and Laaha, G., 2013. Lfstat-low-flow analysis in r. *In*: *EGU General Assembly*
662   *Conference Abstracts*. vol. 15, 7770.

663 Lang, M., *et al.*, 2006. Incertitudes sur les débits de crue. *La Houille Blanche-Revue interna-*
664   *tionale de l'eau*, 6, p–33.

665 Lang, T.J. and Barros, A.P., 2004. Winter storms in the central himalayas. *Journal of Meteo-*
666   *rological Society of Japan*, 82 (3), 829–844.

667 Masson, V., *et al.*, 2003. A global database of land surface parameters at 1-km resolution in
668   meteorological and climate models. *Journal of climate*, 16 (9), 1261–1282.

669 Nepal, S., *et al.*, 2014. Understanding the hydrological system dynamics of a glaciated alpine
670   catchment in the Himalayan region using the J2000 hydrological model. *Hydrological Pro-*
671   *cesses*, 28 (3), 1329–1344.

672 Nepal, S., 2012. *Evaluating upstream-downstream linkages of hydrological dynamics in the hi-*
673   *malayan region*. Thesis (PhD). PhD Thesis. Friedrich Schiller University, Germany.

674 Nepal, S., Flügel, W.A., and Shrestha, A.B., 2014. Upstream-downstream linkages of hydro-
675   logical processes in the himalayan region. *Ecological Processes*, 3 (1), 1.

676 Noilhan, J. and Mahfouf, J.F., 1996. The isba land surface parameterisation scheme. *Global*
677   *and planetary Change*, 13 (1), 145–159.

678 Noilhan, J. and Planton, S., 1989. A Simple Parameterization of Land Surface Processes
679   for Meteorological Models. *Monthly Weather Review*, 117 (3), 536–549. Available from:
680   http://dx.doi.org/10.1175/1520-0493(1989)117¡0536:ASPOLS¿2.0.CO;2.

681 Pellicciotti, F., *et al.*, 2012. Challenges and uncertainties in hydrological modeling of remote
682   hindu kush-karakoram-himalayan (hkh) basins: suggestions for calibration strategies. *Moun-*

tain Research and Development, 32 (1), 39–50.

Pianosi, F., Sarrazin, F., and Wagener, T., 2015. A matlab toolbox for global sensitivity analysis. *Environmental Modelling & Software*, 70, 80 – 85. Available from: http://www.sciencedirect.com/science/article/pii/S1364815215001188.

Pokhrel, B.K., *et al.*, 2014. Comparison of two snowmelt modelling approaches in the dudh koshi basin (eastern himalayas, nepal). *Hydrological Sciences Journal*, 59 (8), 1507–1518.

Ragettli, S., *et al.*, 2015. Unraveling the hydrology of a himalayan catchment through integration of high resolution in situ data and remote sensing with an advanced simulation model. *Advances in Water Resources*, 78, 94–111. Available from: http://linkinghub.elsevier.com/retrieve/pii/S0309170815000159.

Roe, G.H., 2005. Orographic precipitation. *Annu. Rev. Earth Planet. Sci.*, 33, 645–671.

Roocks, P. and Roocks, M.P., 2016. Package rpref.

Salerno, F., *et al.*, 2015. Weak precipitation, warm winters and springs impact glaciers of south slopes of mt. everest (central himalaya) in the last 2 decades (1994–2013). *The Cryosphere*, 9 (3), 1229–1247.

Saltelli, A., *et al.*, 2006. Sensitivity analysis practices: Strategies for model-based inference. *Reliability Engineering & System Safety*, 91 (10), 1109–1125.

Sarrazin, F., Pianosi, F., and Wagener, T., 2016. Global sensitivity analysis of environmental models: Convergence and validation. *Environmental Modelling & Software*, 79, 135 – 152. Available from: http://www.sciencedirect.com/science/article/pii/S1364815216300251.

Savéan, M., 2014. *Modélisation hydrologique distribuée et perception de la variabilité hydroclimatique par la population du bassin versant de la dudh koshi (népal)*. Thesis (PhD). Université de Montpellier 2.

Savéan, M., *et al.*, 2015. Water budget on the Dudh Koshi River (Nepal): Uncertainties on precipitation. *Journal of Hydrology*. Available from: http://linkinghub.elsevier.com/retrieve/pii/S0022169415008082.

Sevruk, B., Ondrás, M., and Chvíla, B., 2009. The wmo precipitation measurement intercomparisons. *Atmospheric Research*, 92 (3), 376–380.

Shrestha, D., Singh, P., and Nakamura, K., 2012. Spatiotemporal variation of rainfall over the central himalayan region revealed by trmm precipitation radar. *Journal of Geophysical Research: Atmospheres*, 117 (D22).

Spear, R. and Hornberger, G., 1980. Eutrophication in peel inletii. identification of critical uncertainties via generalized sensitivity analysis. *Water Research*, 14 (1), 43 – 49. Available from: http://www.sciencedirect.com/science/article/pii/0043135480900408.

Valéry, A., Andréassian, V., and Perrin, C., 2009. Inverting the hydrological cycle: when streamflow measurements help assess altitudinal precipitation gradients in mountain areas. *New approaches to hydrological prediction in data sparse regions. Wallingford: IAHS Press, IAHS Publ*, 333, 281–286. Available from: http://hydrologie.org/redbooks/a333/IAHS3330281.pdf.

Valéry, A., Andréassian, V., and Perrin, C., 2010. Regionalization of precipitation and air temperature over high-altitude catchments learning from outliers. *Hydrological Sciences Journal*, 55 (6), 928–940. Available from: http://dx.doi.org/10.1080/02626667.2010.504676.

World Meteorological Organization, 2008. *Manual on low-flow estimation and prediction*. Geneva, Switzerland: World Meteorological Organization.

Yatagai, A., *et al.*, 2012. Aphrodite: Constructing a long-term daily gridded precipitation dataset for asia based on a dense network of rain gauges. *Bulletin of the American Meteorological Society*, 93 (9), 1401–1415.